Path of magnetic flux lines through high-T_c copper oxide superconductors

Zhen Yao, Seokwon Yoon, Hongjie Dai, Shoushan Fan & Charles M. Lieber*

Division of Applied Sciences and Department of Chemistry, Harvard University, Cambridge, Massachusetts 02138, USA

A SERIOUS impediment to many potential applications of the high-transition-temperature (high-T_c) copper oxide superconductors is the relative ease with which magnetic flux lines move within these materials, thereby producing finite electrical resistance[1,2]. To devise methods for rigidly fixing flux lines in these materials, which is necessary to achieve a truly superconducting (zero resistance) state, requires an understanding of their fundamental properties. In clean, conventional type II superconductors, flux lines or vortices can be modelled well as rigid objects that pass straight through a sample. In the high-T_c materials, however, comparatively short coherence lengths, large anisotropies and large accessible thermal energies lead to more complex and fascinating behaviour, giving for example entangled flux lines and two-dimensional pancake vortices[3–5]. Some detail of the vortex lattice has been resolved previously[6–13], although it is not clear how vortices pass through these materials. Here we address this critical issue by simultaneously decorating the positions of flux lines at opposite sides of single-crystal $Bi_2Sr_2CaCu_2O_8$ (BSCCO) high-T_c superconductors using the Bitter technique[14,15]. These new data enable us to quantify the wandering of vortices as they pass through the BSCCO high-T_c materials and address the elasticity of the vortex lattice. This information will be useful for devising effective strategies for pinning flux lines to the crystal lattice.

Conventionally, the Bitter technique involves decorating individual vortices with small magnetic particles as they emerge from one surface of a superconductor[14,15]. A common weakness of previous decoration studies is, however, their measurement of only a single two-dimensional slice of the vortex lattice at the sample surface[7–10]. Because vortices are believed to be flexible in high-T_c materials and because their interaction at the surface differs from that in the bulk, it is difficult to extrapolate convincingly the three-dimensional properties of the vortex lattice from

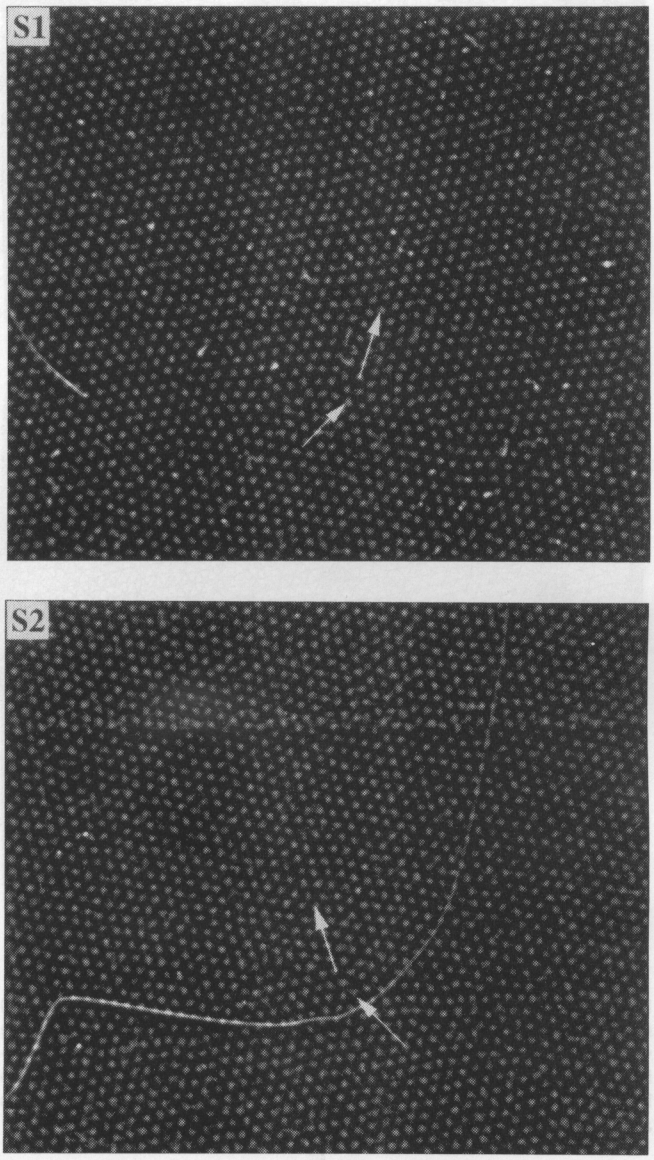

FIG. 1 Scanning electron microscope (SEM) images of side 1 (S1, top) and side 2 (S2, bottom) of a 20-μm-thick BSCCO single crystal decorated with magnetic iron clusters in an applied field of 12 G; S1 and S2 correspond to the same *x–y* spatial location. The white circular spots in these images correspond to the positions of individual vortices. White arrows in S1 and S2 highlight the different vortex lattice orientations on either side of a grain boundary. Images S1 and S2 are both $65.5 \times 56.1\ \mu m^2$ and the lattice constant is 1.4 μm. The BSCCO single crystals (typical size, $2 \times 2 \times 0.02\ mm^3$) were prepared and characterized as described[9]. After cleaving a BSCCO crystal, several hundred ångströms of gold was deposited by sputtering onto each crystal side. Atomic force microscopy showed that the gold films were smooth (<10 nm corrugation) and thus do not affect the vortex lattice. The gold-coated samples were mounted with the magnetic field perpendicular to the BSCCO *a–b* plane, field-cooled to 4.2 K, and then the flux-line positions were decorated with evaporated iron clusters[7,9]. The arrangement of clusters marking the flux-line positions was imaged at room temperature with a scanning electron microscope. Although decoration is at 4.2 K, the resulting flux-line pattern corresponds to the position of vortices frozen at a higher temperature[1,9].

* To whom correspondence should be addressed.

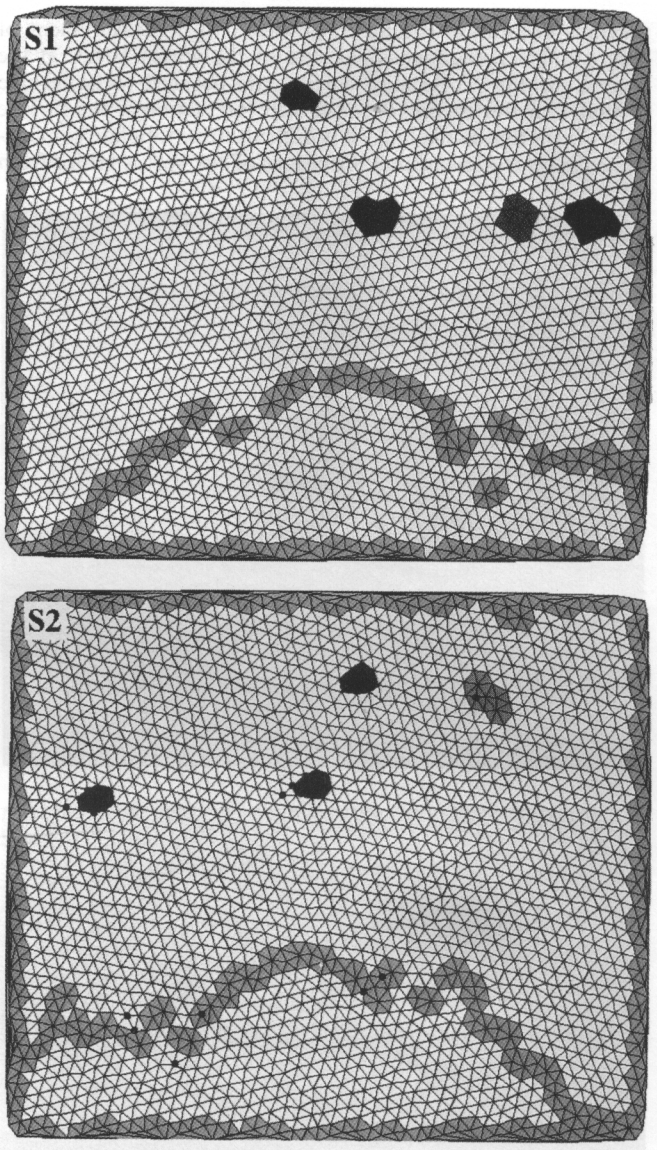

FIG. 2 Delaunay triangulations of the images S1 (top) and S2 (bottom) shown in Fig. 1. In the triangulation, each flux line corresponds to the vertex formed by bonds drawn from the flux line to its n nearest neighbours. Vortices that do not have six nearest neighbours are shaded to highlight their locations in S1 and S2. Apparent extra flux-line positions are indicated by filled black circles on S2.

a single two-dimensional slice[3,16–18]. Significantly, this limitation of the Bitter technique can be overcome simply by decorating both sample sides simultaneously. Correlation of the vortex lattice structures obtained from both sample sides could then be used to address directly the path of vortices through the sample bulk[17].

A conventional arrangement was used to decorate both sample sides (two-sided decoration), except that the two opposing BSCCO a–b plane surfaces are exposed simultaneously to the source of magnetic particles. Because the contact area of the sample with the thermal sink is greatly reduced when both sample sides are exposed, we found it necessary to reduce the sample heating that occurs during the formation of magnetic clusters. This reduction was achieved by coating both sides of the BSCCO samples with several hundred ångströms of gold. Images of the same x–y location on two sides of a decorated BSCCO sample are shown in Fig. 1. The positions of individual vortices appear as small white spots in these images. We were able to image the same x–y location to within ±5 μm by translating the crystal in the microscope a fixed distance from a reference common to both sides of the sample. This positioning uncertainty is close to but greater than the spacing between flux lines; but by matching localized defects in the vortex lattice (that is, grain boundaries), it is possible to register the two images at the level of individual vortices.

The positions of individual vortices on side 1 (S1) and side 2 (S2) of the sample are well resolved in Fig. 1; two-sided decoration images of similar quality were obtained in independent experiments using the procedures described. Several important facts can be gleaned from these two images. First, the two-dimensional vortex lattice structure observed on either S1 or S2 is similar to that reported previously in single-sided decoration experiments (for similar applied fields)[8,9], so we can conclude that the thin gold coating does not affect the observed lattice structure. Second, both S1 and S2 exhibit a grain boundary in the vortex lattice that runs across the lower parts of these images; we highlight the change in lattice direction across the grain boundary using arrows in the images. By placing images S1 and S2 back to back (as they were recorded from the sample), one can see qualitatively that the vortex lattice grain boundaries observed at the two sample sides overlap well and that the lattice orientations in each grain are the same on both sides. Interestingly, we have recently suggested on the basis of single-sided decoration studies of BSCCO that grain boundaries in the vortex lattice should pass through these samples[9,10]. To our knowledge, our two-sided decoration experiments provide the first proof of this proposal.

We have carried out Delaunay triangulations of the Bitter patterns to obtain greater insight into the three-dimensional vortex lattice structure (Fig. 2). The analysis highlights several significant features. First, the grain boundary already discussed (green) is found to consist of alternating 5-coordinate/7-coordinate lattice sites running along the direction of the grain boundary. The similar topology of this extended defect on both S1 and S2 enables us to register the images to much less than a flux-line lattice constant, a_0. Second, isolated topological defects are observed on each side of the sample. Three of these defects, which are highlighted in red, magenta and cyan, are common to both sides of the sample and correspond to dislocations in the vortex lattice. The red dislocation is aligned vertically on S1 and S2, whereas the centres of the magenta and cyan dislocations are displaced with respect to one another. In addition, each side exhibits a topological defect (purple, S1; orange, S2) that does

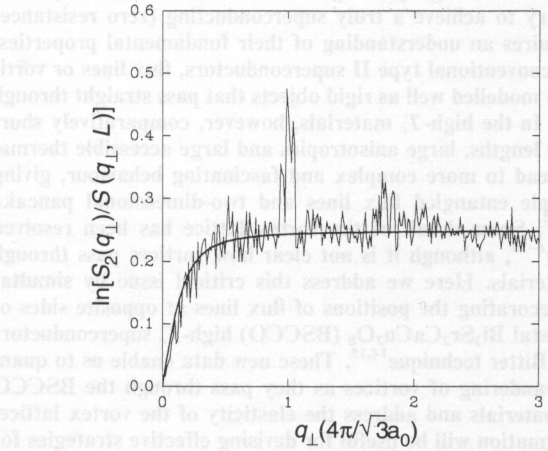

FIG. 3 Plot of $\ln(S_2(q_\perp)/S(q_\perp, L))$ versus $q_\perp$. The solid curve corresponds to a fit of the data using $L \cdot \sqrt{(c_{11}q_\perp^2/c_{44})/[1+q_\perp^2\lambda(T)^2]}$, where $c_{11}/c_{44} = 1.5 \times 10^{-4}$ *and* $\lambda(T) = 1$ μm. Using a value of $\lambda(0) \approx 0.25$ μm and this value of λ, we estimate that the vortices dropped out of equilibrium at $T = 0.98\ T_c$, close to the experimentally observed irreversibility line.

not have a corresponding match on the opposite sample side. The purple defect on S1 is a twisted bond; and probably corresponds to a fluctuation frozen while the sample was cooled before decoration. The orange defect on S2 arises from an interstitial vortex. The observation of these defects implies that at least some vortices wander significantly as they pass through the sample.

This analysis shows that the number of vortices is different on the two sample sides. Extra vortices are highlighted on S2 with solid black dots (Fig. 2). The observation of extra vortices has been confirmed in independent images. These results at first seem remarkable as vortices cannot start or stop within the sample bulk[2]. We believe that the extra vortices can be explained by a small magnetic field inhomogeneity that arises from the non-uniform edges of the BSCCO samples (D. R. Nelson, personal communication). An estimate of this inhomogeneity from the ratio of the number of extra vortice to total vortices yields ~0.6% and is thus quite small. Although the origin of this observation needs to be clarified, our results demonstrate the importance of two-sided decoration in studies of the vortex lattice.

The analysis of topological defects in the vortex lattice at the two sample sides shows that the vortices are flexible and can wander as they pass through the BSCCO samples. We have quantified this wandering by calculating the root-mean-square (r.m.s.) displacement of the flux-line positions $\langle|\mathbf{r}(L)-\mathbf{r}(0)|^2\rangle^{1/2}$, as they cross the sample from S1 ($z=0$) to S2 ($z=L$), where $\mathbf{r}$ is the flux-line position, L is the sample thickness and the brackets signify an average over all vortices (excluding the extra ones) in the images. Our calculations show that $\langle|\mathbf{r}(L)-\mathbf{r}(0)|^2\rangle^{1/2}=0.3$ μm for the 20-μm thick sample discussed, corresponding to a wandering of ~20% of a_0. This r.m.s. displacement is comparable to the Lindemann criteria for melting of a solid lattice and again suggests that there is considerable flux-line wandering within these materials.

To determine whether the observed wandering of vortices through these materials affects the fundamental properties of the vortex array, and thus how it might be pinned, we have evaluated a ratio of the vortex elastic constants. The elastic moduli can be determined from the structure function that describes the vortex density fluctuations as a function of the in-plane ($q_\perp$) and out-of-plane (q_z) wavevectors. Here the flux-line positions have been determined at two discrete out-of-plane positions ($z=0$ and $z=L$, where L is the sample thickness), and in this case the structure function can be written $S(q_\perp, L)=\langle\rho_{q_\perp}(L)\cdot\rho^*_{q_\perp}(0)\rangle$, where $\rho_{q_\perp}$ is the Fourier transform of the vortex density in a given plane. The structure function has been evaluated previously[3,18,19], showing that

$$S(q_\perp, L)=S_2(q_\perp)\exp(-\varepsilon(q_\perp)L/k_BT) \quad (1)$$

where $S_2(q_\perp)$ is computed for a constant z slice ($z=0$ or $z=L$). By treating explicitly the repulsive interaction between vortices

$$\frac{\varepsilon(q_\perp)}{k_BT}\approx\sqrt{\frac{c_{11}q_\perp^2/c_{44}}{1+q_\perp^2\lambda(T)^2}} \quad (2)$$

where c_{11} and c_{44} are the $\mathbf{q}\to 0$ bulk and tilt moduli and $\lambda(T)$ is the temperature-dependent penetration depth (for our magnetic field and sample size, $c_{11}(\mathbf{q})\approx c_{11}/(1+q_\perp^2\lambda^2)$ and $c_{44}(\mathbf{q})\approx$constant[20]). Physically, equations (1) and (2) imply that the decay in flux-line correlations through the sample is governed by the bulk and tilt moduli of the vortices. This model was originally derived for flux liquids, but equation (2) has the same form for a thermally excited crystalline lattice away from the reciprocal lattice vectors, provided $c_{66}\ll c_{11}(\mathbf{q})$ (ref. 19). Hence our analysis is not limited to a particular state of the vortices.

As $S(q_\perp, L)$ and $S_2(q_\perp)$ can be calculated from our two-sided decoration results, it is possible to evaluate readily c_{11}/c_{44} and $\lambda(T)$ from equation (2) (Fig. 3). Several important conclusions can be drawn from these results. First, we find that $\varepsilon(q_\perp)$ goes linearly to zero in the limit $q_\perp\to 0$. This result shows that we are dealing with line-like objects as opposed to two-dimensional pancake vortices[17]. Second, we can fit the experimental data very well over the range of experimentally accessible wavevectors, and thus reliably determine that $c_{11}/c_{44}=1.5\times10^{-4}$ and $\lambda(T)=1$ μm. Significantly, the small value of c_{11}/c_{44} determined in these studies suggests a strong downward renormalization of the bulk modulus from its zero temperature value; that is, the vortex array is much more easily compressed than expected for rigid parallel lines[20]. This strong renormalization cannot be explained by simple crystal defects such as dislocations in a crystalline lattice, but may be due to thermal wandering of vortices from straight trajectories[3,19]. Although more theoretical and experimental work will be needed to understand this fundamental renormalization of c_{11}, we believe that this new information will be useful in devising strategies for effectively pinning vortices and thereby enhancing critical current in the high-T_c materials. □

Received 15 July; accepted 21 September 1994.

1. Bishop, D. J., Gammel, P. L., Huse, D. A. & Murray, C. A. *Science* **255,** 165–172 (1992).
2. Huse, D. A., Fisher, M. P. A. & Fisher, D. S. *Nature* **358,** 553–559 (1992).
3. Nelson, D. R. & Seung, H. S. *Phys. Rev.* B**39,** 9153–9174 (1989).
4. Brandt, E. H. *J. Supercond.* **6,** 201–217 (1993).
5. Clem, J. R. *Phys. Rev.* B **43,** 7837–7846 (1991).
6. Dolan, G. J., Chandrashekhar, G. V., Dinger, T. R., Feild, C. & Holtzberg, F. *Phys. Rev. Lett.* **62,** 827–830 (1989).
7. Grier, D. G. *et al. Phys. Rev. Lett.* **66,** 2270–2273 (1991).
8. Bolle, C. A. *et al. Phys. Rev. Lett.* **66,** 112–115 (1991).
9. Dai, H., Liu, J. & Lieber, C. M. *Phys. Rev. Lett.* **72,** 748–751 (1994).
10. Yoon, S., Dai, H., Liu, J. & Lieber, C. M. *Science* **265,** 215–218 (1994).
11. Cubitt, R. *et al. Nature* **365,** 407–411 (1993).
12. Yethiraj, M. *et al. Phys. Rev. Lett.* **70,** 857–860 (1993).
13. Harada, K. *et al. Phys. Rev. Lett.* **71,** 3371–3374 (1993).
14. Essman, U. & Träuble, H. *Phys. Status Solidi* **18,** 813–828 (1966).
15. Huebner, R. P. *Magnetic Flux Structures in Superconductors* (Springer, Berlin, 1979).
16. Huse, D. A. *Phys. Rev.* B**46,** 8621–8623 (1992).
17. Nelson, D. R. in *Phenomenology and Applications of High-Temperature Superconductors* (eds Bedell, K. S., Inui, M., Meltzer, D., Schrieffer, J. R. & Doniach, S.) 187–242 (Addison-Wesley, New York, 1992).
18. Marchetti, M. C. & Nelson, D. R. *Phys. Rev.* B**47,** 12214–12223 (1993).
19. Nelson, D. R. & Le Doussal, P. *Phys. Rev.* B**42,** 10113–10129 (1990).
20. Fisher, D. S. in *Phenomenology and Applications of High-Tempeature Superconductors* (eds Bedell, K. S., Inui, M., Meltzer, D., Schrieffer, J. R. & Doniach, S.) 287–327 (Addison-Wesley, New York, 1992).

ACKNOWLEDGEMENTS. We thank D. R. Nelson for discussion. C.M.L. acknowledges support of this work by the NSF Division of Materials Research and the Harvard Materials Research Laboratory.